International Journal of Heat and Technology
Vol. 42, No. 6, December, 2024, pp. 1849-1858
Journal homepage: http://iieta.org/journals/ijht

Free Convection inside Greenhouse Cavity Partially Filled with Bottom Porous Layer: The Influence of Soil's Porosity and Permeability

Chihab Eddine Brahmi[1,2*], Mouna Maache Battira[1], Nourredine Belghar[1,3], Mahmoud Kalfali[1], Zied Driss[4]

[1] Mechanical Engineering Department, Science and Technology Faculty, Abbes Laghrour University, Khenchela 40000, Algeria
[2] Laboratoire des Structures, Propriétés et Interactions Interatomiques LASPI2A, Faculté des Sciences et de la Technologie, Université Abbes Laghrour, Khenchela 40000, Algeria
[3] Laboratoire de Génie Energétique et Matériaux, LGEM, University of Biskra, Biskra 07000, Algeria
[4] LASEM Laboratory, National school of Engineering of Sfax (ENIS), University of Sfax, Sfax 3038, Tunisia

Corresponding Author Email: brahmi.chihabeddine@univ-khenchela.dz

https://doi.org/10.18280/ijht.420602

Received: 9 October 2024
Revised: 19 November 2024
Accepted: 26 November 2024
Available online: 31 December 2024

Keywords:
free convection, greenhouse, semi-ellipse, porous layer, porosity, soil, permeability

ABSTRACT

This article presents a geothermal investigation numerically performed on the selection of soils for greenhouses. The primary objective is to analyse the effects of soil properties on heat transfer within greenhouse configurations. Steady free convection phenomenon inside a two-dimensional cavity configuration partially filled from below by a porous layer, and covered by a semi-elliptical upper boundary, mimicking a greenhouse above the soil. The analysis was conducted using the Galerkin finite element technique. The cavity is subjected to a hot isothermal temperature Th along the bottom wall, while a cold temperature Tc is applied to the top wall. To simulate momentum transfer in a porous medium, the Darcy-Brinkman model, due to the non-Darcian flow, is used. This work covered numerous parameters, including Rayleigh numbers (10^4<Ra<10^6), Darcy numbers (10^{-4}<Da<10^{-2}), and porosities (0.3<ε<0.9). Findings show that heat transfer is significantly affected by raising the Rayleigh number. Additionally, the impact of porosity is relatively small, while the rise in permeability through increasing the Darcy number value enhances the heat transfer for high Rayleigh values. In conclusion, the study demonstrates that Rayleigh and Darcy numbers play crucial roles in optimizing heat transfer for greenhouse applications, while porosity has a lesser effect.

1. INTRODUCTION

Aligning with the Algerian government's interest in exploiting its desert soil. Greenhouse farming in these regions presents a promising solution for agriculture in arid areas. However, controlling the essential parameters necessary for the proper functioning of the greenhouse, such as soil quality, moisture content, temperature and others, remains a significant challenge. A lot of researchers have conducted experimental and numerical investigations on greenhouses and related fields, including geothermal, and natural airflow in container homes and constructions. At first, Heat transfer via natural convection processes was their primary area of interest, resulting from the circulation of fluid parts between locations of various temperatures. Driven by buoyancy within various cavities. Their investigations included various heating scenarios, such as in the work of Sathiyamoorthy et al. [1]. Where they applied linear heating, Sivasankaran and Bhuvaneswari [2] used sinusoidal heating from below, studies [3-5] keeping temperature applied isothermally. While Bhardwaj et al. [6] analyze numerically natural convection within irregular cavity shape as Dutta et al. [7] chose quadrantal. Likewise, Brahmi et al. [8] studied entropy generation with free convection inside cavities with irregular vertical walls, besides other researchers [9-12] used simple geometric shapes of cavities as squares, rectangles and triangles.

Among the numerous studies investigating greenhouses, Taloub et al. [13] explored the effect of soils' tilt angles on greenhouse presented by half elliptical cavity shape where results demonstrate that even by a slight inclination altered the motion of the fluid and heat fields, enhancing heat diffusion with greater thermal Rayleigh numbers.

Others were interested in the impact of including porous blocks. According to the research conducted by Belalem et al. [14] experimentally explored the mechanism of free convection within an agricultural greenhouse and numerically by a 2D cavity filled with two rectangles miming porous media, where they concluded that in order to create an optimal environment for tomato growth, it is essential to maintain closed openings, particularly during nighttime, without the necessity of a heating system. Especially for arid climate zones. The free convection in a tube-heated, enclosed model greenhouse with different roof boundary conditions was analyzed in a numerical investigation by Ghernaout et al. [15]. The study analyses heat and fluid flow behavior inside the

greenhouse, including average velocity and temperature, using a CFD algorithm that is employs the finite volume method. Consistent with experimental data, the results show that these factors significantly affect the interior climate of the greenhouse. Additionally, a computational model was created by Raza et al. [16] to examine the microclimatic conditions inside a greenhouse distillation system and find ways to optimize its performance. Temperatures, flow rates, and relative humidity are just a few of the system performance metrics provided, along with recommendations on how to make it even better. While intake velocity and plant transpiration have a substantial effect on relative humidity, the data reveal that a temperature rise of 8°C causes a small drop of around 2%. Zhang et al. [17] performed a numerical investigation interested in developing a mathematical model for 2D heat transfer within a greenhouse air cavity. Factors influencing free convection are inclination angle, number of PV panels and fluid thermo-physical properties. Results determine that as the Rayleigh number (Ra) increases, natural convection intensifies. Additionally, the panel slope angle (θ) significantly affects heat transfer regions, with larger θ leading to a reduced vertical temperature gradient and more uniform temperature distribution. In the investigation conducted by Slatni et al. [18] examined numerical natural heat convection in a closed tunnel greenhouse setting. They assessed the contribution of the Rayleigh number ($Ra=10^3$ to 10^6), as well as the arrangement of tubes was analyzed to investigate their impacts on heat transfer within the greenhouse. As a result, they found that for lower Rayleigh numbers, heat transfer is primarily governed by conduction. As the Rayleigh number and the number of tubes increase, free heat convection mechanism becomes more dominant, leading to enhanced heat transfer.

In recent exploring works on the dynamics of heat transfer in porous materials, Fenni et al. [19] demonstrated that natural convection in a square cavity with a porous layer at the bottom is significantly influenced by Darcy numbers and porosity. Higher Darcy numbers and porosity were found to enhance heat transfer by facilitating fluid flow and increasing the heat exchange surface area, whereas thicker porous layers reduced heat transfer due to increased resistance to fluid flow and decreased heat exchange contact area. Building on this, Barman and Srinivasa Rao [20] investigated local thermal non-equilibrium conditions in a porous enclosure with a wavy cold side wall using the Galerkin finite element method. Their analysis focused on parameters such as interface heat transfer coefficient, porosity, Rayleigh-Darcy number, and cavity waviness. The study revealed that increased waviness improves heat transfer between the fluid and solid phases, with local thermal equilibrium conditions varying based on specific parameter configurations. Together, these works provide valuable insights into optimizing heat transfer performance in porous systems by accounting for material, structural, and flow characteristics. According to the study by Kumar et al. [21], the performance of two solar dryers, the forced convection greenhouse dryer (FCGHD) and the forced convection cabinet solar dryer (FCCSD), was experimentally compared under the climatic conditions of Hisar, India. Their findings showed that the FCCSD was significantly more efficient, exhibiting 55.2% higher drying efficiency and 37.87% lower specific energy consumption compared to the FCGHD. This enhanced performance was further supported by the Midilli–Kucuk model, which proved effective in modeling the drying behavior of date fruits. Such advancements in drying systems align with the need for improved environmental control in agricultural applications. Similarly, Velasco et al. [22] analyzed a greenhouse-type solar coffee dehydrator, comparing natural and forced convection methods. The use of forced convection powered by photovoltaic energy reduced drying time from three and a half days to two and a half days, achieving a moisture reduction from 52% to 12% on a wet basis. While natural convection resulted in higher air temperatures (60-70°C), forced convection operated at slightly lower temperatures (50-60°C) while maintaining coffee quality. This balance between energy input and drying performance mirrors the efficiency gains observed in FCCSD systems, emphasizing the critical role of controlled convection in agricultural applications. Expanding on the relationship between system geometry and heat transfer, Paing and Anderson [23] investigated how aspect ratio and roof pitch influence natural convection heat transfer in closed even-span gable-roof greenhouses. Their results, supported by CFD and experimental data, revealed that reducing the aspect ratio and roof pitch could decrease natural convection heat transfer by up to 25% and 15%, respectively. However, in certain conditions, these geometrical changes induced multicellular flow regimes, which increased heat transfer instead. Furthermore, Tawfik et al. [24] proposed a controlled natural convection (CNC) solar greenhouse dryer (SGD) as a cost-effective solution for drying grapes. By combining the simplicity of natural convection (NC) and the efficiency of forced convection (FC), the CNC mode reduced moisture content from 5.91 g water/g dry matter to 0.15 g within 12 hours, outperforming the NC mode, which required 15 hours. The CNC mode also achieved higher thermal efficiency (12.5%) and the lowest drying cost (1.26 USD/kg), with a payback period of just 1.08 years.

Our study introduces a novel fusion of diverse research elements, through the study of heat transfer phenomena within agricultural greenhouses. By introducing natural convection inside a cavity constrained by an upper half-elliptical shaped wall, partially filled with a porous layer from below to mimic soil under the greenhouse, investigating how soil permeability and porosity and varying Rayleigh numbers on thermal and flow characteristics inside greenhouse environments. The soil beneath the greenhouse can be altered by removing unsuitable soil and replacing it with a soil mixture that has a better water-holding capacity. And retain nutrients, as the greenhouse will protect them from erosion. This research promises to revolutionize greenhouse exploitation and farming practices, and offers insights to enhance productivity and sustainability across crops in arid desert regions.

2. COMPUTATIONAL MODEL DESCRIPTION

2.1 Physical model configuration

Figure 1 illustrates the configuration under study, consisting of a greenhouse cavity partially filled by a porous layer from below. The cavity was heated from below by exposing the bottom wall of the porous layer to an isothermal hot temperature Th. While along the upper semi-elliptical wall remains cold, keeping vertical walls adiabatic.

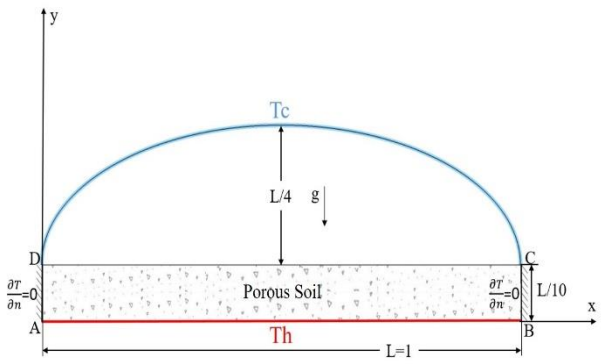

Figure 1. Current problem model

2.2 Mathematical formulation

The flow model is based on the following key assumptions: the fluid is Newtonian, steady, laminar, and incompressible, with a two-dimensional inviscid flow. All thermophysical properties, except for density, are assumed to be constant. Density variations in the body force term are modeled using the Boussinesq approximation. Momentum transfer within the porous layer is described by the Darcy-Brinkman-Forchheimer extended model. Additionally, local thermal equilibrium is assumed. The governing mass, momentum, and energy equations for free convection in this model are expressed in non-dimensional form as follows [3, 5]:

The dimensionless equations for the porous layer, derived from the extended Darcy-Brinkman model, are given as:

Continuity equation:

$$\frac{\partial \mathrm{U}}{\partial \mathrm{X}}+\frac{\partial \mathrm{V}}{\partial \mathrm{Y}}=0 \tag{1}$$

Momentum along the X-axis:

$$\begin{aligned}&\frac{1}{\varepsilon}\left[U\frac{\partial}{\partial X}\left(\frac{U}{\varepsilon}\right)+V\frac{\partial}{\partial Y}\left(\frac{U}{\varepsilon}\right)\right]\\&=-\frac{1}{\varepsilon}\frac{\partial\left(\varepsilon P_f\right)}{\partial X}+\frac{Pr}{\varepsilon}\left(\frac{\partial^2 U}{\partial X^2}+\frac{\partial^2 U}{\partial Y^2}\right)\\&-U\frac{Pr}{Da}-\frac{1.75}{\sqrt{150}}\frac{U\sqrt{(U^2+V^2)}}{\sqrt{Da}\cdot\varepsilon^{3/2}}\end{aligned} \tag{2}$$

Momentum along the Y-axis:

$$\begin{aligned}&\frac{1}{\varepsilon}\left[U\frac{\partial}{\partial X}\left(\frac{V}{\varepsilon}\right)+V\frac{\partial}{\partial Y}\left(\frac{V}{\varepsilon}\right)\right]\\&=-\frac{1}{\varepsilon}\frac{\partial\left(\varepsilon P_f\right)}{\partial Y}+\frac{Pr}{\varepsilon}\left(\frac{\partial^2 V}{\partial X^2}+\frac{\partial^2 V}{\partial Y^2}\right)\\&-V\frac{Pr}{Da}-\frac{1.75}{\sqrt{150}}\frac{V\sqrt{(U^2+V^2)}}{\sqrt{Da}\cdot\varepsilon^{3/2}}+RaPr\,\theta\end{aligned} \tag{3}$$

Energy equation:

$$\mathrm{U}\frac{\partial \theta}{\partial \mathrm{X}}+\mathrm{V}\frac{\partial \theta}{\partial \mathrm{Y}}=\mathrm{R_k}\left(\frac{\partial^2 \theta}{\partial \mathrm{X}^2}+\frac{\partial^2 \theta}{\partial \mathrm{Y}^2}\right) \tag{4}$$

For the fluid region, the governing equations are:
Continuity equation:

$$\frac{\partial \mathrm{U}}{\partial \mathrm{X}}+\frac{\partial \mathrm{V}}{\partial \mathrm{Y}}=0 \tag{5}$$

Momentum along the X-axis:

$$U\frac{\partial U}{\partial X}+V\frac{\partial U}{\partial Y}=\frac{\partial P}{\partial X}+Pr\left(\frac{\partial^2 U}{\partial X^2}+\frac{\partial^2 U}{\partial Y^2}\right) \tag{6}$$

Momentum along the Y-axis:

$$U\frac{\partial V}{\partial X}+V\frac{\partial V}{\partial Y}=\frac{\partial P}{\partial Y}+Pr\left(\frac{V}{\partial X^2}+\frac{\partial^2 V}{\partial Y^2}\right)+RaPr\,\theta \tag{7}$$

Energy equation:

$$U\frac{\partial \theta}{\partial X}+V\frac{\partial \theta}{\partial Y}=\frac{\partial^2 \theta}{\partial X^2}+\frac{\partial^2 \theta}{\partial Y^2} \tag{8}$$

Local Nusselt number:

$$\mathrm{Nu}=-\frac{\partial \theta}{\partial \mathrm{n}} \tag{9}$$

where, ∂/∂n denotes the non-dimensional derivative in the direction perpendicular to the surface in consideration and the l below represents the length of the wall.

Average Nusselt number:

$$Nu_{avg}=\frac{1}{l}\int_0^l Nu\,dx \tag{10}$$

The subsequent boundary conditions listed below are applied to solve the equations:

$$\mathrm{U}=\mathrm{V}=0 \text{ and } \theta=1 \text{ along (AB)} \tag{11a}$$

$$\mathrm{U}=\mathrm{V}=0 \text{ and } \mathrm{n}\frac{\partial \theta}{\partial \mathrm{n}}=0 \text{ along (AD and BC)} \tag{11b}$$

$$\mathrm{U}=\mathrm{V}=0 \text{ and } \theta=0 \text{ along the curved wall (CD)} \tag{11c}$$

The horizontal boundary (DC), separating the fluid from the porous layer involves both flow and heat transfer phenomena. For the flow across this interface, specific conditions are imposed to regulate the interaction between the two regions. The conditions of velocity, temperature, normal stress and heat flux continuities at the interface are as follow [5]:

$$\overrightarrow{U}|_{fluid}=\overrightarrow{U}|_{porous}=\overrightarrow{V}|_{interface} \tag{11d}$$

$$\overrightarrow{\theta}|_{fluid}=\overrightarrow{\theta}|_{porous}=\overrightarrow{\theta}|_{interface} \tag{11e}$$

$$\frac{1}{\varepsilon}\frac{\partial U_n}{\partial n}\Big|_{porous}=\frac{\partial U_n}{\partial n}\Big|_{fluid} \tag{11f}$$

$$\mathrm{R_k}\frac{\partial \theta}{\partial \mathrm{n}}\Big|_{\mathrm{porous}}=\frac{\partial \theta}{\partial \mathrm{n}}\Big|_{\mathrm{fluid}} \tag{11g}$$

3. NUMERICAL SIMULATION

We have used COMSOL Multiphysics ®, a commercial

software based on the finite element technic. The governing Equations, including the set of boundary conditions, were treated. Where the mesh inside the computational model follows a triangular grid, we use the weak form of the governing equations using the (GFEM) Galerkin finite element method. Velocity components and pressure are Discretized choosing P2–P1 Lagrange finite elements with Lagrange-quadratic finite elements for the temperature.

3.1 Grid sensitivity test and validation

In order to inspect mesh quality, we were assessed the average Nusselt number for the free convection within the greenhouse along the bottom wall. Where, the cavity is subjected to a constant heating from below, while the upper wall maintains cold and keeps vertical walls adiabatic. With fixing the set of parameters on ($Ra=10^6$, $Da=10^{-2}$, $\varepsilon=0.9$ and $Pr=0.71$). Table 1 presents the mesh-density test for the greenhouse cavity, which compared several meshes for the greenhouse cavity model of various numbers of elements. From the findings of our study, we obtained a converged solution for the meshes, we selected a mesh density of 37400 elements to achieve accurate faster solution computation.

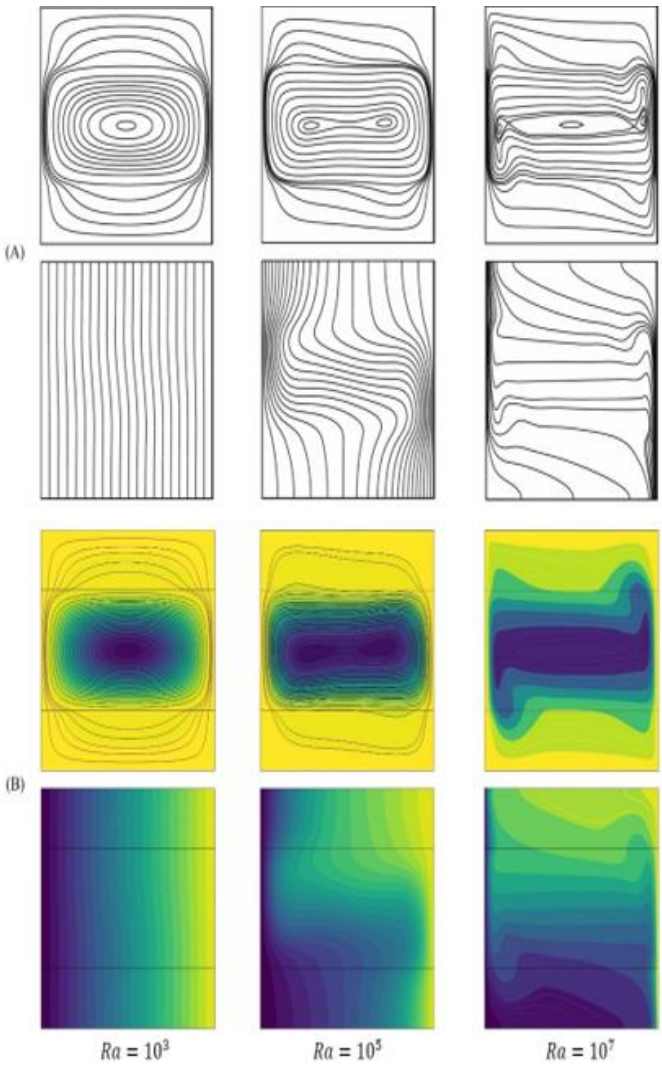

Figure 2. Comparative evaluation of results from (A) Chen et al. [5] and (B) the current study, showing streamlines in the upper panels and isotherms in the lower panels for A=0.25, $Da=10^{-4}$, $\varepsilon=0.4$

Table 1. Results of the dependency test on the mesh at $Ra=10^6$, $Da=10^{-2}$, $\varepsilon=0.9$ and $Pr=0.71$

Mesh	5228	12744	20154	37400	55268
Nu_{avg}	10.130	10.882	10.902	11.061	11.063

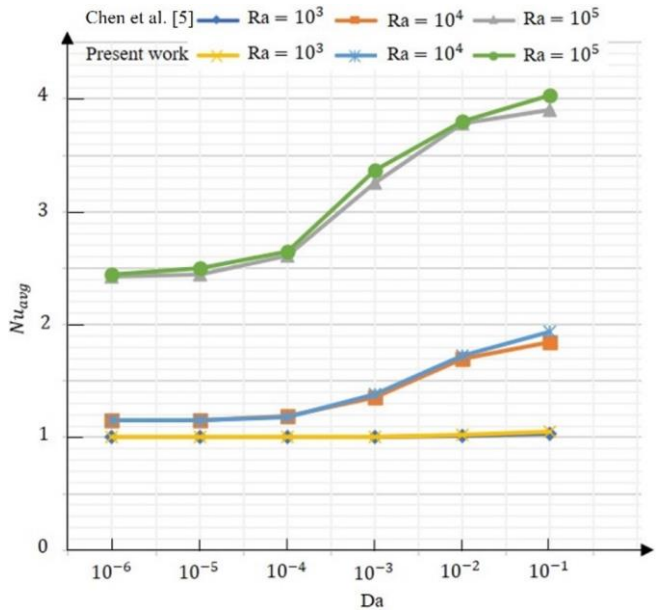

Figure 3. Results comparison of current test side by side to those of Chen et al. [5] of Nu_{avg} on the left side wall at various combinations of (Da and Ra) for a/L=0.25, $\varepsilon=0.4$

To evaluate the accuracy of the commercial CFD software. Employed in the current study findings have been evaluated and compared by the investigation of Chen et al. [5]. For a bidimensional square cavity of length L=1, partially filled by two horizontal porous layers placed at both the upper and lower walls of the cavity, where they have same thickness L/4, the cavity cooled from left side wall and heated from right while keeping others adiabatic, the flowing fluid has a Prantld number Pr=1, The porous layers have a porosity of $\varepsilon=0.4$. In Figure 2, the streamlines and isotherms at Darcy number ($Da=10^{-4}$) are compared and the results are closely aligned with those of Chen et al. [5]. Moreover, a comparison of the average Nusselt numbers obtained for several Rayleigh and Darcy numbers matches the findings presented in the same study (see Figure 3).

The chosen ranges for Rayleigh numbers, Darcy numbers, and porosities reflect realistic scenarios commonly encountered in greenhouse applications, ensuring practical relevance. The numerical technique, specifically the Galerkin finite element method, was selected for its proven accuracy and effectiveness in solving convection and heat transfer problems.

Rayleigh Numbers ($10^4<Ra<10^6$): This range was chosen to capture the behavior of natural convection across varying intensities, with lower values representing stable convection and higher values highlighting enhanced heat transfer mechanisms. Darcy values between (10^{-4} and 10^{-2}). Indeed; we conducted the study within the range of (10^{-4} to 10^{-2}) to explore various scenarios encompassing both low and high permeability conditions. The selected range represents typical permeability values of porous medium (soil) used in greenhouse applications. This approach allows us to gain insights into how different permeability conditions affects our

results, providing a comprehensive understanding of the system's behavior. Regarding the selection of porosity ($0.3<\varepsilon<0.9$), typical soil porosity (ε) ranges between 0.2 and 0.6, representing denser to moderately permeable soils. However, higher porosity values (ε), such as 0.9, were included in the analysis to explore scenarios with extreme permeability, such as highly porous substrates or engineered soils, which are sometimes used in advanced greenhouse applications to optimize aeration and drainage. This extended range ensures the study covers a broad spectrum of practical and theoretical conditions, providing a comprehensive understanding of the system's thermal behavior.

4. RESULTS AND DISCUSSION

This study thoroughly explores the impact of how changes in the Rayleigh number (Ra, from 10^3 to 10^6), Darcy number (Da, from 10^{-4} to 10^{-2}), and porosity (ε, 0.3 0.6. 0.9). On isotherms, streamlines and local Nusselt number (Nu) variation. The investigation is particularly focused on air as acting fluid, where Prandtl number (Pr=0.71).

4.1 Streamlines and isothermal contours

In order to elucidate the heat transfer and fluid flow behaviors across different porosities values, Rayleigh and Darcy numbers, a comprehensive analysis of flow and thermal fields is indispensable. Figures 4-7 illustrate how the isotherms and streamlines patterns within the enclosure are affected by different Darcy (Da) numbers, Rayleigh (Ra) numbers and porosities (ε). It's evident that regardless of the values of (Da, Ra, and ε), two similar spinning vortices form within the cavity, rotating in opposite directions to each other within the cavity. Due to the imposed boundary conditions (see Figures 5 and 7).

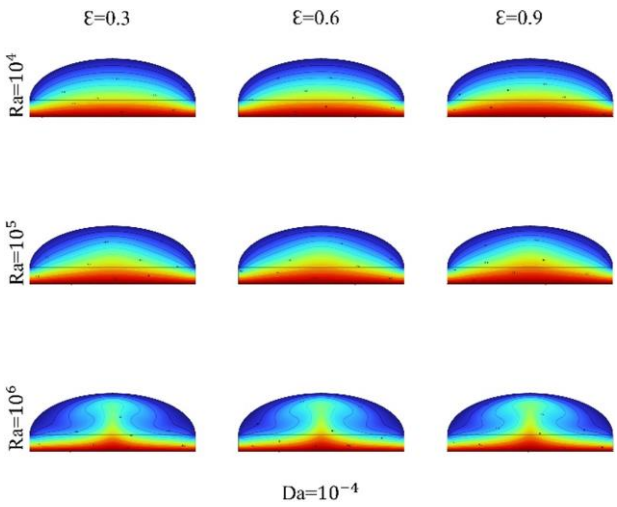

Figure 4. Isotherms corresponding to a set of porosities and Rayleigh numbers at $Da=10^{-4}$

In the case of the lower Darcy number ($Da=10^{-4}$) for Ra up to 10^5 and all porosities values, Figure 5 shows the flow structure formed by two weak symmetrical eddies. Due to the fact that at this level of ($Da=10^{-4}$) the permeability is low where the effect of porosity remains negligible, unlike for ($Ra=10^6$), The intensity of the eddies increases because of the augmentation of buoyancy force. On the other hand, when ($Da=10^{-2}$), (see Figure 7) for small ($Ra=10^4$) and various porosities, the fluid remains motionless which can be explained by the weak of buoyancy force and the high flow resistance. When the Rayleigh number reaches ($Ra=10^5$), the rotating vortices enhanced and at this level the effect of porosity starts acting where the higher porosity facilitates fluid motion more than smaller values, upon reaching a ($Ra=10^6$), the flowing eddies increased strongly to reach high values for the three porosities but it gets its maximal values in case of porosity ($\varepsilon=0.9$).

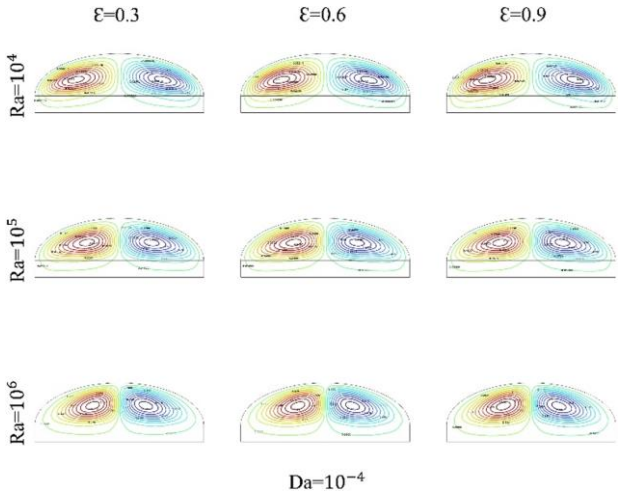

Figure 5. Streamlines corresponding to a set of porosities and Rayleigh numbers at $Da=10^{-4}$

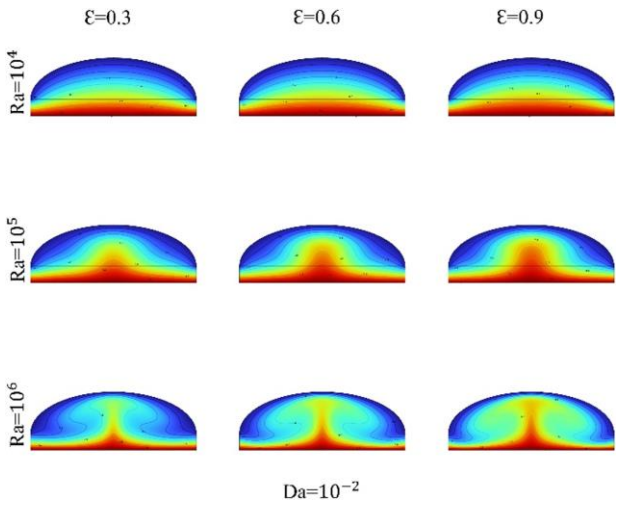

Figure 6. Isotherms corresponding to a set of porosities and Rayleigh numbers at $Da=10^{-2}$

Figures 4 and 6 showcase the contour of isotherms for lower and higher Darcy number values respectively. For the various porosities set. The top panels in these figures illustrate a smooth distribution of isotherms throughout the cavity, forming arc-like patterns centered by the midpoint of the heated bottom wall. This is due to the low Rayleigh number value ($Ra=10^4$), which implies a uniform isothermal distribution resulting from weak convective heat transfer. The dominance of heat conduction over convection in this scenario is attributed to the resistance forces due to fluid viscosity being much greater than the buoyant forces driving convection. Consequently, heat transfer occurs predominantly through conduction, as fluid friction impedes the formation of strong

convective currents.

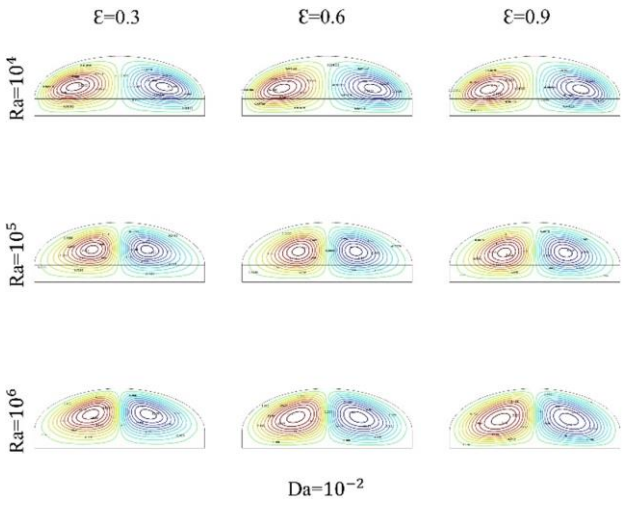

Figure 7. Streamlines corresponding to a set of porosities and Rayleigh numbers at $Da=10^{-2}$

In Figure 4, when the Rayleigh value is ($Ra=10^5$), it was noticeable that along the mid-section of panels, the distribution of isotherms becomes increasingly sharper with higher porosity values, where transitioning from smooth arcs to more sharp patterns within the cavity. This is attributed to can be explained by the superiority of the buoyancy force over the force due to fluid friction being. Then by raising the Rayleigh number to ($Ra=10^6$). The isotherms distribution exhibits as a symmetrical plume pattern intense slightly as porosity increases. Due to enhanced convection strength, the primary mechanism of thermal energy transport within the enclosure shifts to convection. In Figure 6, as the (Ra) is increased to ($Ra=10^5$), we observe that the thermal field contour transitions from an arc shape to a wave-like form in the cavity's center. this wave is strengthened by rising porosity value. As buoyancy increases proportionally with flow motion through highly permeable porous media. Buoyancy, driven by density gradients, becomes more pronounced as permeability increases, allowing fluid to flow more freely through the porous structure. In addition, at the highest value of ($Ra=10^6$), the isotherms take on a fountain-like shape. The isotherms take on a fountain-like shape, promoting the acceleration of the particles toward the elliptical wall. While noting the porosity's impact strength at this level, where the illustration clearly depicts a notable variation between the smallest and highest porosity value. As a result of several causes. Firstly, an increase in the Darcy number signifies higher permeability, indicating reduced resistance to fluid flow through the porous layer. This is due to the larger void spaces within the medium, allowing fluid to flow more easily. Secondly, a rise in the (Ra) indicates a stronger dominance of buoyancy forces over other forces like viscosity within the fluid. Lastly, an increase in porosity means there are more open voids within the porous layer, decreasing the obstacles to fluid flow and reducing flow resistance. At this level the convection mode is the dominant.

4.2 Local Nusselt number

Figures 8 and 9 illustrate the evolution of the local Nusselt number along the heated bottom wall beneath the porous layer and the upper cooled wall, respectively. These figures highlight the impacts of various porosities, Rayleigh numbers, and Darcy numbers on heat transfer characteristics.

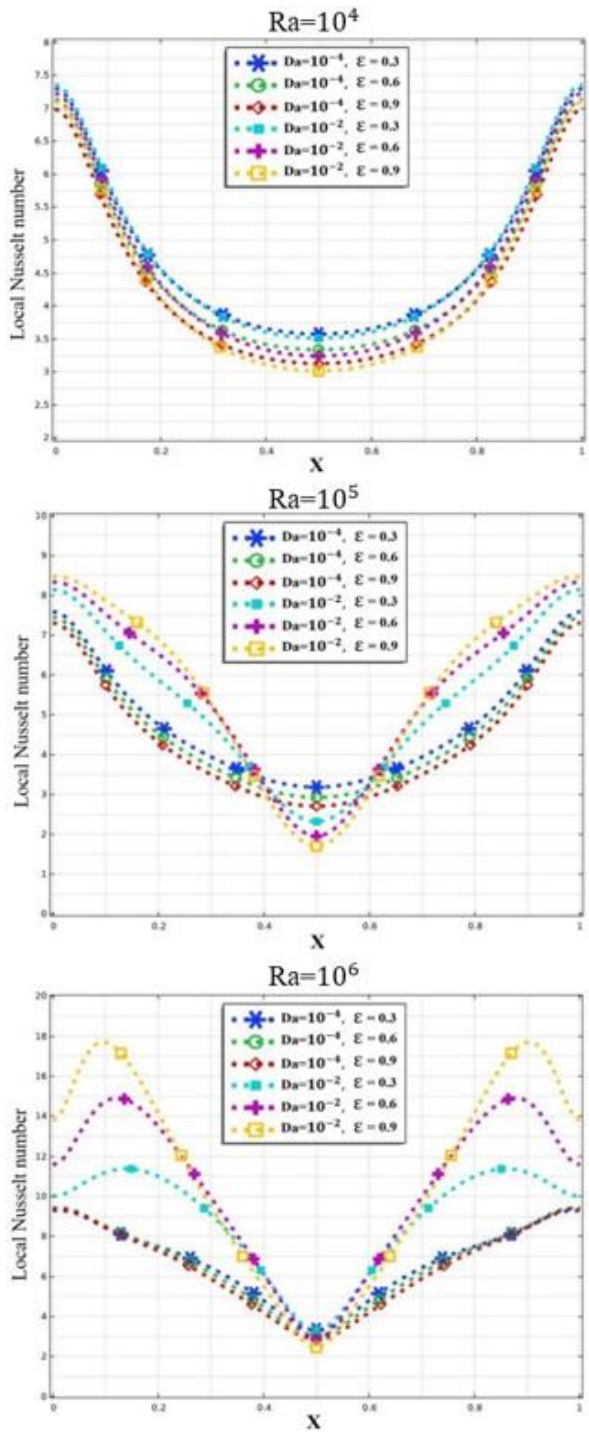

Figure 8. Nu along the heated wall with different combinations of porosities, Rayleigh numbers and Darcy numbers

Figure 8 shows that, at a low Rayleigh number value of $Ra=10^4$, the evolution of the Nusselt number (Nu) exhibits an arc-shaped pattern across all curves. High Nu values appear at both ends of the bottom cavity wall, followed by a symmetrical decline towards the center of the bottom hot wall around X=0.5, where it reaches its lowest value of Nu=3. This value corresponds to the highest porosity and Darcy number. After reaching this minimum, Nu begins to increase again due to the consistent thermal behavior along the heated wall. This behavior can be attributed to the weak influence of the low Rayleigh number on the various permeabilities and porosities, resulting from moderate and insignificant temperature differences across the fluid, leading to weak convection.

Additionally, at this level of Rayleigh number, the findings show only slight differences in Nu between high and low Darcy numbers for each porosity. When the porosity (ε) increases from 0.3 to 0.9, Nu shows a modest decrease in the central region, suggesting that lower porosity values slightly enhance convective heat transfer.

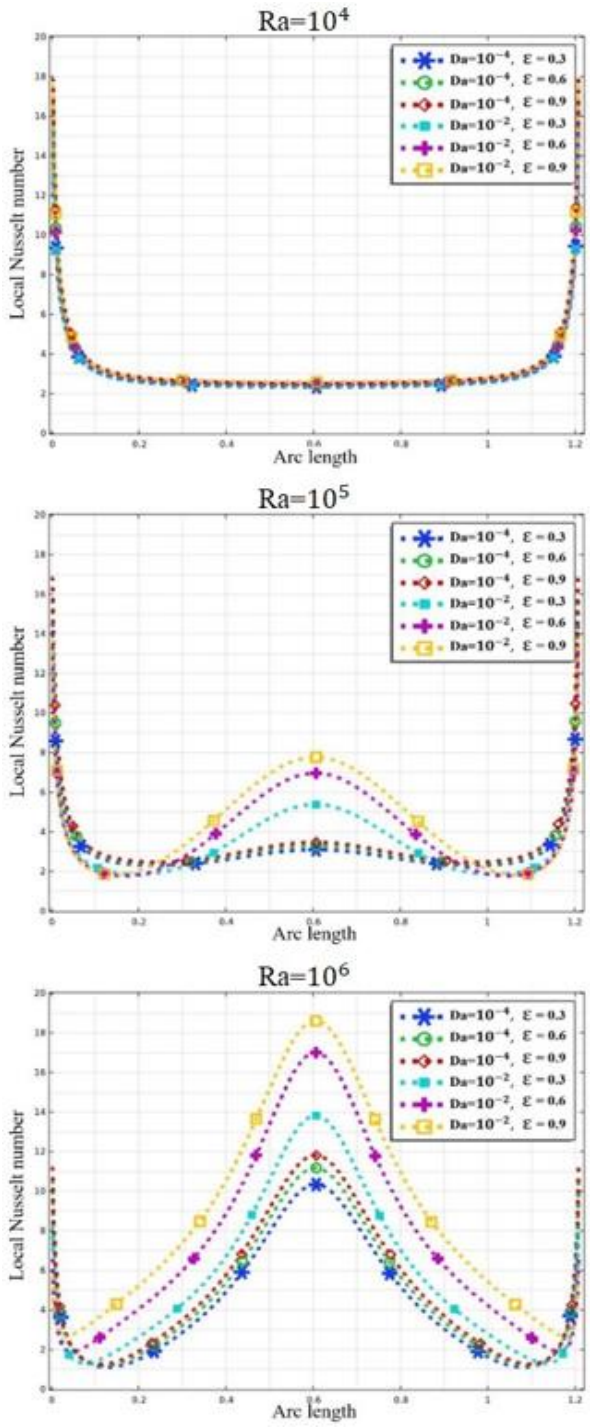

Figure 9. Nu along the cooled wall with different combinations of porosities, Rayleigh numbers and Darcy numbers

For $Ra=10^5$, the Nu curves transition from an arc-like shape at low Darcy numbers ($Da=10^{-4}$), which closely resembles the behavior observed with $Ra=10^4$, to a V-like shape at high Darcy numbers ($Da=10^{-2}$). This indicates that the Rayleigh effect becomes more dominant at higher permeability ($Da=10^{-2}$) while having minimal impact at low permeability ($Da=10^{-4}$). The increased permeability associated with higher Darcy values enhances the buoyancy force, which drives stronger convection. Across all porosities, the Nu curves remain close to each other for any Darcy value, indicating that changes in porosity have minimal impact. At $Da=10^{-2}$ and a porosity of ε=0.9, the Nu reaches its highest values (8.5) in the corners of the bottom wall and decreases to Nu=1.8 in the central region. This behavior occurs because the buoyancy force outweighs the friction force, particularly at high permeability.

When the Rayleigh number increases to $Ra=10^6$, the Nu curves continue to exhibit a V-like trend for $Da=10^{-4}$, with curves remaining uniformly close for all porosities. However, for $Da=10^{-2}$, the curves shift to a wavier form, reaching higher values in the left and right regions. At this stage, the Nu increases and then decreases in a V-like manner. The effect of porosity becomes more significant at this level. For the lowest porosity (ε=0.3), the Nu starts at 10 and increases to 11.4, while for the highest porosity (ε=0.9), the Nu starts at 14 and reaches 17.7. This behavior is due to the increasing dominance of the buoyancy force over the viscous force as the Rayleigh number, porosity, and permeability increase, allowing fluid particles to flow more freely. This results in enhanced heat transfer, primarily driven by convection as the dominant mechanism. A decrease in Nu is noticeable in the middle region, which is attributed to the boundary condition applied to the upper wall.

Figure 9 shows the distribution of the (Nu) along the upper cold wall, for a minor ($Ra=10^4$), the variation of the (Nu) along the upper cooled half-elliptical wall follows the same trend qualitatively and quantitatively, for all values of the Darcy numbers and porosities. This can be explained by the relatively weak impact of buoyancy force despite varying permeabilities and porosities. For ($Ra=10^5$), curves of (Nu) distribution for small Darcy value ($Da=10^{-4}$) keep the same distribution of ($Ra=10^4$), with negligible variation.

Due to the low permeability which restricts the fluid motion. For ($Da=10^{-2}$), (Nu) displays elevated values at the right and left corners. It then decreases sharply. Subsequently, it rises towards the central region. The physical reason for the increased heat transfer within the cavity is the high permeability and the rise in porosity, which creates more voids for particles to flow through. Improving the heat transfer process by convection. When the Rayleigh number reaches ($Ra=10^6$), the buoyancy force is significantly enhanced. As a result, Nu shows high values at the corners, which then decreases owing to weak flow in those areas. Following this, increases along the central zone, where it peaks higher values by rising Darcy number, attributable to the fact that the permeability increases with higher values of (Da). Which is also proportional to increasing porosity, further enhancing the effect. Due to the previously stated reasons.

The present study's findings align well with previous research. To provide a comprehensive perspective, the findings of the current investigation are compared with those of Chen et al. [5]. Reveals various similarities and distinctions in the analysis of heat transfer and fluid flow in porous media. Both studies emphasize the influence of the Darcy number (Da) on fluid motion and heat transfer, with a decrease in (Da) increasing the resistance of the porous medium and suppressing convection. In the current investigation, for ($Da=10^{-4}$), the flow remains weak at low (Ra) due to limited permeability, which aligns with findings [5], that for ($Da=10^{-5}$), the porous medium behaves almost like a solid,

restricting convection and resulting in conduction-dominated heat transfer. Both works also highlight the transition from conduction-dominated to convection-dominated regimes with increasing (Ra), as buoyancy-driven convection intensifies. In the present work, higher (Ra) values ($Ra=10^5$) and ($Ra=10^6$) deform isotherms and enhance flow motion, comparable to Chen et al. [5], who report similar trends for (Ra) values up to (10^7). Additionally, the effect of porosity (ε) on fluid motion and heat transfer is consistently observed in both studies. In the current investigation, higher porosity (ε) facilitates fluid flow, reduces resistance, and enhances convection, which corresponds to findings [5], that increased permeability due to higher (Da) or porosity (ε) supports more vigorous fluid motion. Both studies also underline the role of (Da) in affecting local heat transfer rates, with reduced (Da) leading to smaller local Nusselt numbers and weaker convection. However, there are notable differences. Furthermore, Chen et al. [5] examine a broader range of (Da) values (10^{-6}) to (10^{-1}) and include detailed Nusselt number behavior, showing a stop increasing as (Da) decreases further below (10^{-5}). Due to conduction dominance, whereas the current investigation focuses on specific values ($Da=10^{-4}$) and ($Da=10^{-2}$), where selected range represents typical permeability values of porous medium (soil) used in greenhouse applications. and provides qualitative insights into isotherm and streamline transitions. Despite these differences, both works converge on the fundamental impact of (Da), (Ra), and (ε) on heat transfer and flow dynamics within porous media.

4.3 Average Nusselt number

Figure 10 depicts the evolution of the average Nusselt number along the bottom wall and the half-elliptical upper wall for different values of porosity, Rayleigh numbers and Darcy numbers. It is important to note that at a low value of ($Da=10^{-4}$), for the lower value of ($Ra=10^4$), the Nu_{avg} on both the bottom and upper walls remains unaffected by the Darcy number, while the influence of porosity is slightly notable, it is clear from (Figure 10(a)) that the increase in porosity is causing a decrease in Nu_{avg} along the hot wall. Which is the opposite of the case on the upper wall, where Nu_{avg} increases by a small incrementation proportional to the augmentation of the porosity value, due to the fact that increasing pores make the fluid flow more freely. Thus, the (Da) has negligible impact on the heat transfer characteristics at this level of the (Ra). As the Rayleigh number reaches ($Ra=10^5$), the Nu_{avg} along the bottom and upper wall exhibit the same behavior at first, moving in a straight or approximately constant manner. This is because a low Darcy value indicates low permeability that led to the dominance of frictional force over buoyancy force. When the (Ra) increases further to ($Ra=10^6$), the curves rise, where the effect of porosity remains almost unchanged, due to the buoyancy force exceeding the viscous force, the Rayleigh number has a virtual influence on the heat transfer characteristics, where the mechanism of heat transfer is convection. However, as the Darcy number increased to ($Da=10^{-2}$), it can be observed from (Figure 10(a)), When ($Ra=10^4$), that the Nu_{avg} influenced by porosity value, and the highest porosity proportional to the smallest value of the Nu_{avg}, when Rayleigh number up to ($Ra=10^5$), the curves upward while inversing the impact of porosity, because at higher permeability ($Da=10^{-2}$) the fluid flow easily and the buoyancy force sharply dominate viscous force. As the (Ra) increased to ($Ra=10^6$), a strong upward, at this level of Rayleigh number the effect of the Darcy number and the porosity value is largely notable, which can be explained by the dominance of the buoyancy force, making heat transfer occur entirely through convection. (Figure 10(b)) demonstrates the variations of the Nu_{avg} along the upper cold wall, for ($Ra=10^4$) the values of the Nu_{avg} remain small, enhanced as the (Ra) increased further, to get its higher value for the higher porosity. Due to the same physics mentioned above.

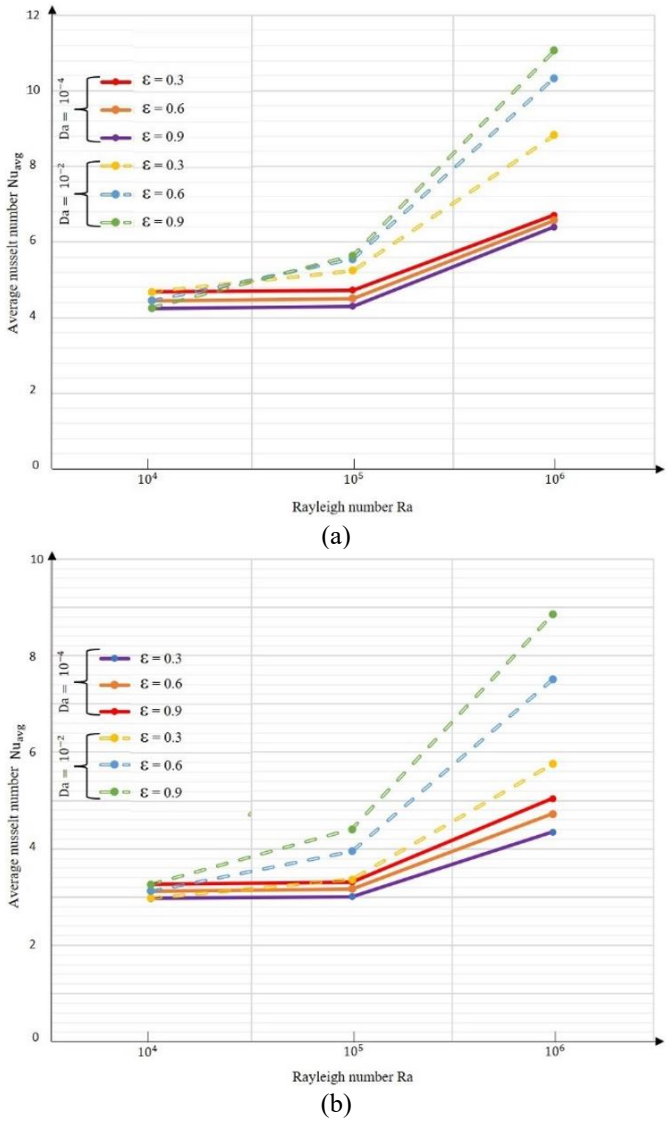

Figure 10. Dependence of Nu_{avg} r along (a) bottom and (b) upper wall on different porosities, Rayleigh numbers and Darcy numbers

5. CONCLUSIONS

In conclusion, our study has conducted a comprehensive numerical investigation of free convection inside a greenhouse cavity partially filled by a porous layer from the bottom to mimic the soil, by varying the considered parameters: (Ra, Da, and porosity (ε)). The obtained findings show that the local Nusselt numbers along the heated bottom wall, for low Darcy number ($Da=10^{-4}$) indicate that increasing the Rayleigh number greatly affects heat transfer. This demonstrates that at low permeability, the dominant heat transfer mechanism is conduction, with convection being less pronounced even as (Ra) increases. Additionally, the impact of porosity (ε) is relatively small and opposite, where increasing porosity

decreases the heat transfer on the heated bottom wall. This behavior highlights the resistance introduced by the porous structure, which dampens convective effects at low (Da). This is the opposite of the case on the upper wall, where the (Nu_{avg}) increases by a small incrementation proportional to the augmentation of the porosity (ε) value. On the other hand, the highest Darcy value ($Da=10^{-2}$) leads to enhancing the buoyancy with respect to increasing Rayleigh number and dominance of the mechanism of heat transfer into convection. Under these conditions, the porous medium allows for stronger fluid motion, with buoyancy-driven convection becoming the dominant mechanism. At this level of Darcy number, the porosity (ε) effect is considerable, as increasing porosity significantly enhances the heat transfer with each level of Rayleigh number value. This implies that for high permeability (Da) and porosity (ε), the porous medium facilitates efficient thermal regulation, making it particularly suitable for arid climate applications.

•The findings suggest that using highly permeable soil layers with higher porosity (ε) for greenhouses in arid climates, can enhance heat dissipation.

•The results show that porosity (ε) plays a dual role: inhibiting heat transfer at low (Da) but facilitating convection at higher (Da), which offers a pathway to customize soil layers for specific thermal needs.

•Investigate the interaction of transient thermal loads, such as diurnal temperature cycles, on the heat transfer mechanisms observed in this study.

•Extend the analysis to experimental validation using real-world greenhouse setups to confirm the numerical predictions.

•Explore the coupling of free convection with forced ventilation systems to develop hybrid thermal management strategies.

REFERENCES

[1] Sathiyamoorthy, M., Basak, T., Roy, S., Pop, I. (2007). Steady natural convection flow in a square cavity filled with a porous medium for linearly heated side wall(s). International Journal of Heat and Mass Transfer, 50(9-10): 1892-1901. https://doi.org/10.1016/j.ijheatmasstransfer.2006.10.010

[2] Sivasankaran, S., Bhuvaneswari, M. (2013). Natural convection in a porous cavity with sinusoidal heating on both sidewalls. Numerical Heat Transfer, Part A: Applications, 63(1): 14-30. https://doi.org/10.1080/10407782.2012.715985

[3] Nithiarasu, P., Seetharamu, K.N., Sundararajan, T. (1997). Natural convective heat transfer in a fluid saturated variable porosity medium. International Journal of Heat and Mass Transfer, 40(16): 3955-3967. https://doi.org/10.1016/s0017-9310(97)00008-2

[4] Basak, T., Kaluri, R.S., Balakrishnan, A.R. (2012). Entropy generation during natural convection in a porous cavity: Effect of thermal boundary conditions. Numerical Heat Transfer, Part A: Applications, 62(4): 336-364. https://doi.org/10.1080/10407782.2012.691059

[5] Chen, X.B., Yu, P., Sui, Y., Winoto, S.H., Low, H.T. (2009). Natural convection in a cavity filled with porous layers on the top and bottom walls. Transport in Porous Media, 78: 259-276. https://doi.org/10.1007/s11242-008-9300-2

[6] Bhardwaj, S., Dalal, A., Pati, S. (2015). Influence of wavy wall and non-uniform heating on natural convection heat transfer and entropy generation inside porous complex enclosure. Energy, 79: 467-481. https://doi.org/10.1016/j.energy.2014.11.036

[7] Dutta, S., Biswas, A.K., Pati, S. (2018). Natural convection heat transfer and entropy generation inside porous quadrantal enclosure with nonisothermal heating at the bottom wall. Numerical Heat Transfer, Part A: Applications, 73(4): 222-240. https://doi.org/10.1080/10407782.2018.1423773

[8] Brahmi, C.E., Maache Battira, M., Belghar, N., Kalfali, M., Bessaih, R. (2024). Free convection and entropy generation inside porous cavities with irregular vertical walls nonuniformly heated from below. Numerical Heat Transfer, Part A: Applications. https://doi.org/10.1080/10407782.2024.2359046

[9] Ma, Z.S., Duan, L.B., Yao, S.G., Jia, X.W. (2015). Numerical study of natural convection heat transfer in porous media square cavity with multiple cold walls based on lBM. International Journal of Heat and Technology, 33(4): 69-76. http://doi.org/10.18280/ijht.330409

[10] Al-Farhany, K., Abdulkadhim, A. (2018). Numerical investigation of conjugate natural convection heat transfer in a square porous cavity heated partially from left sidewall, International Journal of Heat and Technology, 36(1): 237-244. https://doi.org/10.18280/ijht.360132

[11] Triveni, M.K., Panua, R. (2017). Numerical analysis of natural convection in a triangular cavity with different configurations of hot wall. International Journal of Heat and Technology, 35(1): 11-18. https://doi.org/10.18280/ijht.350102

[12] Abdulkadhim A., Abed A.M., Mohsen A.M., Al-Farhany K. (2018). Effect of partially thermally active wall on natural convection in porous enclosure. Mathematical Modelling of Engineering Problems, 5(4): 395-406. https://doi.org/10.18280/mmep.050417

[13] Taloub, D., Bouras, A., Driss, Z. (2020). Effect of the soil inclination on natural convection in half-elliptical greenhouses. International Journal of Engineering Research in Africa, 50: 70-78. https://doi.org/10.4028/www.scientific.net/jera.50.70

[14] Belalem, M.S., Elmir, M., Tamali, M., Mehdaoui, R., Missoum, A., Chergui, T., Bezari, S. (2021). Numerical and experimental study of natural convection in a tunnel greenhouse located in South West Algeria (Adrar region). International Journal of Heat and Technology, 39(5): 1575-1582. https://doi.org/10.18280/ijht.390520

[15] Ghernaout, B., Attia, M.E., Bouabdallah, S., Driss, Z., Benali, M.L. (2020). Heat and fluid flow in an agricultural greenhouse. International Journal of Heat and Technology, 38(1): 92-98. https://doi.org/10.18280/ijht.380110

[16] Raza, S.S., El Kadi, K., Janajreh, I. (2018). Greenhouse microclimate flow simulation: Influence of inlet flow conditions. International Journal of Thermal & Environmental Engineering, 17(1): 11-18. https://doi.org/10.5383/ijtee.17.01.002

[17] Zhang, Y., Zhang, M., Xiong, J., Mao, G., Qi, Y. (2023). Computational fluid dynamics for cavity natural heat convection: Numerical analysis and optimization in greenhouse application. Advances in Mathematical Physics, 2023(1): 1074719.

https://doi.org/10.1155/2023/1074719
[18] Slatni, Y., Djezzar, M., Messai, T. (2021). Numerical investigation of natural convection with heated tubes in tunnel greenhouse. Journal of Thermal Engineering, 7(4): 731-745. https://doi.org/10.18186/thermal.915149
[19] Fenni, M., Guellal, M., Hamimid, S. (2024). Influence of porosity properties on natural convection heat transfer in porous square cavity. Physics of Fluids, 36(5): 056108. https://doi.org/10.1063/5.0206797
[20] Barman, P., Srinivasa Rao, P. (2024). Numerical analysis of local thermal non-equilibrium free convection in a porous enclosure with a wavy cold side wall. Proceedings of the Institution of Mechanical Engineers, Part E: Journal of Process Mechanical Engineering, 238(1): 372-382. https://doi.org/10.1177/09544089231154363
[21] Kumar, M., Shimpy, Sahdev, R.K., Sansaniwal, S.K., Bhutani, V., Manchanda, H. (2023). Experimental forced convection greenhouse and indirect cabinet drying of date fruits: A comparative study. Journal of Thermal Analysis and Calorimetry, 148(12): 5437-5454. https://doi.org/10.1007/s10973-023-12057-9
[22] Velasco, O.L., La Madrid, R., Marcelo-Aldana, D., Palacios, J.D. (2023). A comparative energy analysis of natural convection and forced convection in a solar greenhouse coffee dehydrator. In 2023 IEEE Colombian Caribbean Conference (C3), Barranquilla, Colombia, pp. 1-5. https://doi.org/10.1109/c358072.2023.10436308
[23] Paing, S.T., Anderson, T.N. (2024). Characterising the effects of geometry on the natural convection heat transfer in closed even-span gable-roof greenhouses. Thermal Science and Engineering Progress, 48: 102408. https://doi.org/10.1016/j.tsep.2024.102408
[24] Tawfik, M.A., Oweda, K.M., Abd El-Wahab, M.K., Abd Allah, W.E. (2023). A new mode of a natural convection solar greenhouse dryer for domestic usage: Performance assessment for grape drying. Agriculture, 13(5): 1046. https://doi.org/10.3390/agriculture13051046

NOMENCLATURE

Da	Darcy number
g	Gravitational acceleration, $m.s^{-2}$
K	Permeability
L	Length of the greenhouse cavity
Nu	Local Nusselt number
P	Dimensionless pressure
Pr	Prandtl number
Ra	Rayleigh number
R_k	Ratio of thermal conductivity between porous and fluid regions
T	Temperature, K
U, V	Dimensionless velocity components
X, Y	Dimensionless cartesian coordinates

Greek symbols

ε	Porosity
Θ	Dimensionless temperature
ρ	Density, $kg.\ m^{-3}$

Subscripts

avg	Average
c	Cold
f	Fluid
h	Hot
k	Thermal conductivity ($W.m^{-1}.K^{-1}$)
p	Porous media